一种T6态Al-13.0Si-0.7Mg合金的焊接性分析

滕莹雪[1]， 张玉岐[2]， 郭 菁[1]， 杨春利[2]
(1. 辽宁科技大学 材料与冶金学院，鞍山 114001;
2. 哈尔滨工业大学 先进焊接与连接国家重点实验室，哈尔滨 150001)

摘 要： 分别采用ER4047和ER5183焊丝对T6态的Al-13.0Si-0.7Mg合金进行平板对接试验，为了降低热输入的影响，使用双脉冲MIG双面焊成形工艺，确定了两种焊丝对应的焊接工艺参数并且获得了良好的焊缝成形. 鱼骨状热裂纹试验说明该种合金及两种焊丝对该合金的抗热裂性能良好. 在此基础之上，对焊接接头进行金相组织观察和力学性能测试. 结果表明，两种焊丝对应的焊接接头显微组织的差别较大；拉伸试验表明两种焊丝的接头强度为母材的70%左右，显微硬度测试结果表明焊缝热影响区存在软化现象.

关键词： Al-13.0Si-0.7Mg合金；鱼骨状裂纹试验；显微组织；力学性能
中图分类号： TG 406 **文献标识码：** A **文章编号：** 0253-360X(2014)10-0105-04

0 序 言

铝硅合金由于具有高的比强度、密度低、良好的铸造性能、优异的耐磨性和低线膨胀系数等特点而被广泛应用于发动机活塞、缸体、轮辐等零件中，在汽车制造和航空航天等领域应用前景十分广阔[1,2]. 然而铝硅合金随着硅含量的增加，在铸件中会得到粗大的块状硅颗粒和板条形的共晶组织，致使高硅铝合金的塑形下降，不适合作为变形合金使用，从而大大限制了该类型合金的应用[3]. Al-12.7Si-0.7Mg含镁高硅变形铝合金是最近开发成功的[4]，其T6状态的合金与目前广泛应用的6063铝合金相比，具有优异的力学性能，因此极具市场应用前景[5]. 然而目前铝硅合金的焊接问题没有得到很好的解决，主要依靠铸造的方法来制造其结构件，而通常需要连接的部位也采用铆接工艺[6]. 如果能找到满足该类型合金焊接性能要求的焊材和焊接工艺势必会为这种铝合金的推广带来重要的意义.

1 试验方法

由于T6态的铝合金在焊接热循环的作用下，接头会存在严重的软化现象[7]，因此试验为了降低对母材的热输入，提高接头的抗拉强度，采用双面焊接工艺，所用焊机型号为KempArc pulse 450. 母材为200 mm×120 mm×6 mm的T6态Al-13.0Si-0.7Mg合金，开X形坡口，坡口角度为90°，焊接时两坡口间隙为1 mm左右. 根据母材含有元素种类及含量，选择应用广泛的4×××和5×××系列的ER4047和ER5183两种焊丝，直径均为1.2 mm，母材和焊丝的化学成分如表1所示.

表1 母材和焊丝的化学成分(质量分数，%)

Table 1 Chemical compositions of base metal and welding wire

	Cu	Mg	Mn	Si	Fe	Zn	Ti	Al
母材	—	0.62	—	13.13	0.14	—	—	余量
ER4047	0.3	0.10	0.15	11~13	0.80	0.20	—	余量
ER5183	0.1	4.3~5.2	0.5~1.0	0.40	0.40	0.25	0.15	余量

焊前用刮刀严格清理坡口及工件表面的氧化膜，并用丙酮擦拭干净，然后分别使用两种焊丝对板材进行焊接.

对焊接接头金相组织的观察在OLYMPUS-PMG3型金相显微镜下进行，使用电子万能材料试验机INSTRON-5569对焊接接头进行拉伸性能测试(拉伸速率为1 mm/min)，采用HVS-1000数字显微硬度仪对焊接接头进行维氏硬度测试，试验采用鱼骨状可变拘束热裂纹试验方法评定合金的热裂性，鱼骨状试件如图1所示.

2 试验结果与分析

2.1 抗裂性试验

试验采用鱼骨状可变拘束热裂纹试验方法，使用手工钨极氩弧焊，焊接交流电流为110 A，焊接速

收稿日期：2013-12-21

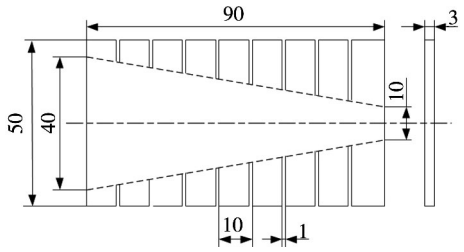

图 1 鱼骨状试件示意图(mm)

Fig. 1 Schematic of fish-bone specimen

度 150 ~ 180 mm/min,在带有铜垫板的专有夹具上施焊,焊接方向为拘束度大处向拘束度小处,进行 3 组试验,其中一组为不填焊丝,其它两组分别添加 ER4047 和 ER5183 焊丝,每组试验重复 3 次.

图 2 为焊后试件对比,可以看出,3 种情况均未产生热裂纹,弧坑处也未出现弧坑裂纹,说明该含镁高硅铝合金以及两种焊丝对该合金具有很好的抗热裂性. 在该铝合金中,由于含有较高的硅含量,可以形成较多的 Al-Si 低熔点共晶,在凝固过程中产生"自愈合"效应[8],而且硅可以改善合金的流动性,并且硅可以降低铝合金的线膨胀系数,从而也降低了热裂倾向,因此该种合金不易产生热裂纹,具有很好的抗热裂纹性能.

(a) 无焊丝 (b) ER4047 (c) ER5183

图 2 鱼骨状可变拘束热裂纹试验试件

Fig. 2 Specimens of fish-bone cracking test

2.2 焊接工艺参数及焊缝成形

表 2 为的两种焊丝双面焊接工艺对应的焊接工艺参数,试验 1,2 分别对应焊丝 ER4047 和 ER5183. 在选取的焊接工艺参数下,获得了成形连续、美观的焊缝.

表 2 焊接工艺参数

Table 2 Welding parameters

试验编号	焊接次序	氩气流量 q/(L·min^{-1})	电弧电压 U/V	焊接电流 I/A	焊接速度 v_1/(mm·s^{-1})	送丝速度 v_2/(mm·s^{-1})
1	第 1 面	23	19.6	121	550	5.3
	第 2 面	23	20.8	128	550	5.6
2	第 1 面	25	18.8	111	550	7.1
	第 2 面	25	19.3	116	550	7.4

2.3 金相组织分析

根据母材的化学成分及他人的研究结果[1,5]可知,母材由 α-Al,Si,Mg_2Si 和含铁相所组成. 但由于 Mg 和 Fe 元素含量较少,因此 Mg_2Si 和含铁相可以忽略掉,母材的 XRD 分析结果如图 3 所示,主要为铝和硅两相所组成.

图 4 为使用两种焊丝对应接头的金相组织形貌. 可以看出,由于焊丝 ER4047 含有的 Si 元素为 11% ~13%,与 Al-Si 共晶点相近,接头的焊缝组织(图 4a)中有较多黑色区域的 Al-Si 共晶组织,白色

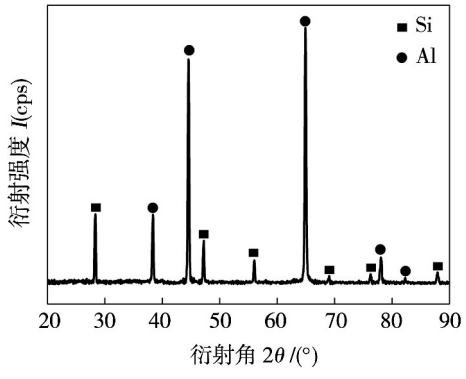

图 3 母材 XRD 分析结果

Fig. 3 XRD analysis of base metal

区域为 α-Al 树枝晶; 而熔合区(图 4b) 冶金结合良好,焊缝金属沿着熔合线向焊缝中心以联生方式长大,熔合线处的 α-Al 枝晶组织较为粗大,靠近熔合线的热影响区组织由于受到较大的热输入影响,硅颗粒发生聚集粗化; 热影响区组织为灰色的硅颗粒弥散分布于 α-Al 固溶体基体上,与母材组织相比,其中的硅颗粒分布较稀疏. 而焊丝 ER5183 对应接头的焊缝微观组织形貌与 ER4047 相差较大,主要是由于 ER5183 焊丝的硅含量较少,所形成的铝硅共晶组织较少,焊缝区内主要由较多的等轴 α-Al 晶粒以及在晶界分布的 Al-Si 共晶组织组成,由于焊丝成分与母材成分在 Si 元素含量上相差较大,在熔合区存在一过渡区域,冶金结合不好,晶粒间结合不紧密,且在熔合线附近的晶粒尺寸较大,这种组织会

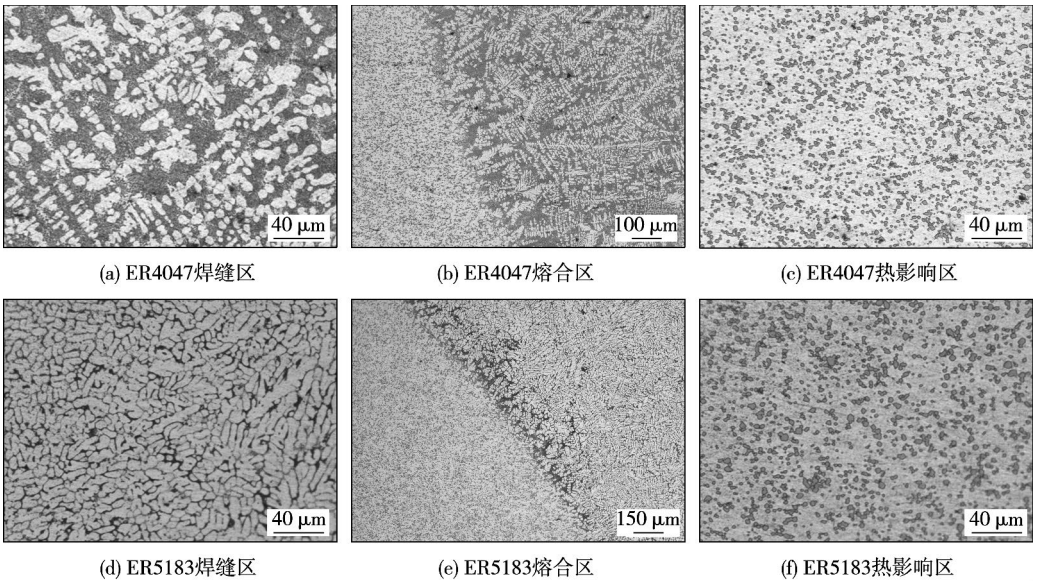

(a) ER4047焊缝区　(b) ER4047熔合区　(c) ER4047热影响区

(d) ER5183焊缝区　(e) ER5183熔合区　(f) ER5183热影响区

图 4　使用两种焊丝的接头显微组织形貌

Fig. 4　Microstructure of joints with two welding wires

对其力学性能带来不利影响.

2.4　力学性能分析

2.4.1　拉伸试验

沿着垂直于焊缝方向进行切割制取拉伸试样,每种试验制取至少 3 个试件(去除余高) ,并用砂纸打磨光滑,两种焊丝的焊接接头拉伸性能如图 5 所示. 使用焊丝 ER4047 的接头抗拉强度平均为 230.1 MPa,达到母材抗拉强度的 70.4%,而焊丝 ER5183 的接头抗拉强度平均为 220.6 MPa,为母材的 67.5%. 焊接接头的断裂位置为靠近焊缝的热影响区和焊缝两种位置,其中断裂在热影响区的原因是母材为 T6 态(固溶处理后人工时效) 经过热处理强化后的材料,其强化机理为铝基体的细晶强化,硅颗粒的颗粒强化和第二相粒子(Mg_2Si) 的沉淀强化[4],受到焊接热源较大的热输入后,热影响区的组织和性能在高温的影响下发生变化,近焊缝的热影响区温度高于原始的固溶温度,使时效析出的 Mg_2Si 强化粒子固溶到 α-Al 基体中,导致强化效果降低,又由于受到较大的热输入后晶粒粗化,使细晶强化作用弱化,导致强度系数降低,虽然采用了双面焊工艺使热输入较单面焊双面成形工艺低,但在焊接热处理强化的铝合金时接头软化现象的存在是 MIG 焊接中不可避免的.

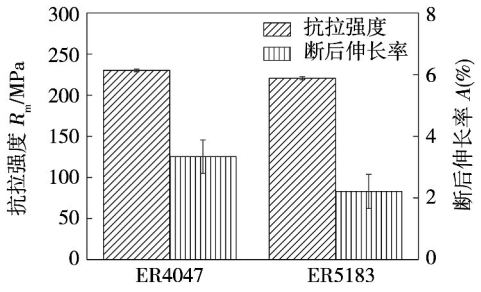

图 5　不同焊丝接头的拉伸性能

Fig. 5　Tensile properties of joints with different fillers

焊接接头的断裂位置在焊缝处具有不同的断裂模式,焊丝 ER4047 的起裂位置在接头焊缝表面处,接头熔合区结合良好,接头断裂在强度相对较弱的焊缝; 而焊丝 ER5183 的接头起裂位置为坡口中心处靠近熔合线附近的焊缝处,虽然 ER5183 熔敷金属的理论强度比较高,但由于母材含有的硅含量较

多，使焊缝的硅含量增加，在熔合区附近冶金结合不良(图4e)，另一方面，焊接过程中 ER5183 焊丝中的 Mg 元素易于烧损以及母材对焊缝金属的稀释作用(能谱测试表明 Mg 元素含量由焊丝的 4.3% ~ 5.2% 降低到焊缝的 1.52% ~ 1.99%)，焊缝中起强化作用的 Mg 元素含量会减少，因此导致接头强度比理论值低.

2.4.2 显微硬度分析

对两种接头进行维氏硬度测试，载荷为 1.96 N，持续时间为 10 s，在焊缝及熔合线附近相邻两个测量点间距为 0.5 mm，其余间隔为 1 mm，从焊缝中心向母材方向进行测试.

图6为焊接接头的显微硬度测试结果. 两种焊丝对应的焊接接头的显微硬度变化趋势相同，都是母材显微硬度最高，而在热影响区硬度明显下降，即接头软化现象，其中使用 ER4047 焊丝的焊缝硬度较 ER5183 焊丝的焊缝硬度值低，由图4a，d 对比可以看出，ER5183 焊丝形成的焊缝组织晶界较多，而晶界对位错运动会有阻碍作用，从而表现为硬度值较高.

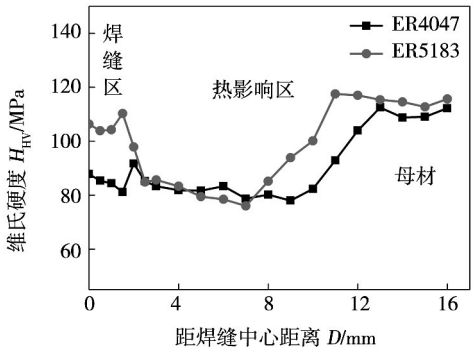

图6 焊接接头的显微维氏硬度

Fig. 6 Hardness value of welded joints

3 结 论

(1) 鱼骨状裂纹试验结果显示该种铝合金和两种焊丝对该合金均未产生热裂纹，抗热裂纹性能好.

(2) 两种焊丝的接头显微组织不同，ER4047 焊丝对应的接头中焊缝组织主要由 Al-Si 共晶和 α-Al 树枝晶组成，在熔合区冶金结合良好; ER5183 焊丝对应的接头焊缝组织主要为 α-Al 等轴晶和在晶界分布的 Al-Si 共晶，在熔合区冶金结合不良.

(3) 拉伸试验表明使用两种焊丝的接头强度为母材的 70% 左右; 显微硬度试验说明接头热影响区存在软化区域.

参考文献:

[1] Cao F, Li Z, Zhang N, *et al*. Superplasticity, flow and fracture mechanism in an Al-12.7Si-0.7 Mg alloy [J]. Materials Science and Engineering: A, 2013, 571(1): 167 - 183.

[2] Xiu Z Y, Chen G Q, Wang X F, *et al*. Microstructure and performance of Al-Si alloy with high Si content by high temperature diffusion treatment [J]. Transactions of Nonferrous Metals Society of China, 2010, 20(11): 2134 - 2138.

[3] 张伟华，邱小明，孙大千，等. ZL109 铝硅合金 CO_2 激光焊接头组织与性能 [J]. 焊接学报，2010，31(6)：45 - 48.
Zhang Weihua, Qiu Xiaoming, Sun Daqian, *et al*. Microstucture and mechanical properties of CO_2 laser-welded joint of ZL109 aluminum silicon alloy [J]. Transactions of the China Welding Institution, 2010, 31(6): 45 - 48.

[4] Zuo L, Yu F, Zhao G, *et al*. A structural material part of a high-Si Mg-containing Al alloy and the manufacture method thereof: United States, 2009003365 [P]. 2009 - 01 - 09.

[5] Liu F, Yu F, Zhao D, *et al*. Microstructure and mechanical properties of an Al-12.7Si-0.7 Mg alloy processed by extrusion and heat treatment [J]. Materials Science and Engineering: A, 2011, 528(10): 3786 - 3790.

[6] 马晓红. 铝硅合金的激光焊接 [D]. 长春：吉林大学，2012.

[7] 朱 亮，龙 林，乔及森. 时效对 6063 铝合金焊接接头性能的影响 [J]. 焊接，2006(5)：26 - 29.
Zhu Liang, Long Lin, Qiao Jishen. Effects of aging on the properties of 6063 Al alloy welded joints [J]. Welding & Joining, 2006(5): 26 - 29.

[8] 严 铿，叶友利，王锡岭. 焊接材料对喷射成形 7475 铝合金 TIG 焊接头热裂纹的影响 [J]. 焊接学报，2012，33(1)：9 - 12.
Yan Keng, Ye Youli, Wang Xiling. Effects of welding materials on hot crack of spray formed 7475 aluminum alloy in TIG welding joint [J]. Transactions of the China Welding Institution, 2012, 33(1): 9 - 12.

作者简介：滕莹雪，女，1979 年出生，博士，高级工程师. 主要从事铝合金材料的开发和性能研究工作. 发表论文 10 余篇. Email: yxteng@imr.ac.cn

of Mechanical & Electronic Engineering, China University of Petroleum, Qingdao 266555, China). pp 93 – 96

Abstract: Based on SYSWELD software, a method verified the parameters of heat source and heat input of double ellipsoid mode and two principles guiding how to determine the above parameters were put forward. Through taking the above mentioned measures, the trailing problem of molten pool rear in Guassian and double ellipsoid mode had been successfully solved. The experimental results show that the predicted shape and trend fusion line on top surface and cross section are in agreement with the experimental measurements. It provides theoretical basis and basic data for precise modeling and intelligent control of TIG welding process. The reason why so marked difference between the predicted and practical trend fusion line at the rear of the pool exists was analyzed, which could provide a guide for the future research.

Key words: double ellipsoid heat source; molten pool geometry; finite element method; gas tungsten arc welding; rear trailing of molten pool

Quantitative analysis of solder powder particle based on morphology LU Lin[1,2], SUN Jia[1], WANG Hongmei[1], WANG Liqiang[3] (1. School of Chemical Equipment, Shenyang University of Technology, Shenyang 111003, China; 2. State Key Laboratory of Advanced Welding and Joining, Harbin Institute of Technology, Harbin 150001, China; 3. University of Dayton, Dayton 45469, America). pp 97 – 100

Abstract: Description and statistical analysis to solder powder particle shape, which is made by ultrasonic atomization, have performed by using morphological methods since high angularity of solder powder particle and less regular shape which are key factors affecting the quality of solder paste preparation. Two important characteristics of solder powder particle shape, solder powder particle fractal dimension and aspect ratio, have been established. Firstly, the geometric projection image of solder powder particle was calculated, and then corrosion and expansion methods of morphology to characterize solder powder particle profiles were done. Moreover, the pattern information on the particle number and radius were statistically calculated. Finally fitting equation with fractal dimension was built. The experimental results showed that the morphological methods submitted by this article can be applied to segmentation adhesion welding particle image. In addition, the aspect ratio and fractal dimension of solder powder particle accurately reflect the solder powder particle real shape.

Key words: lead-free solder powder particles; fractal dimension; image processing; corrosion transformation; dilatation transformation

Analysis on welding porosity of iron powder electrode YIN Shike[1], WU Shuxiong[2], WANG Yong[1], WANG Yishan[1] (1. China Iron and Steel Research Institute Group, Beijing 100081, China; 2. Beijing Miller Electric MFG. Co. Ltd., Beijing 100023, China). pp 101 – 104

Abstract: To determine the nature of the porosity, the gas compositions in porosity were tested by suspension melting-gas chromatography apparatus. The photograph of internal porosity was also observed by SEM. The analysis result shows that the gas compositions of porosity are the same mixed ones of CO and H_2 in both basic and acid electrodes. CO may be considered to play an important role in the formation of porosity. Two kinds of shapes are shown in the interior porosity. The one is worm-like porosity which situated in the middle and upper weld metal, and the other is conchoidal porosity which can be found at the root pass. The analysis result also shows that, whether the formation of porosity or nat, can be predicted by the diffusible hydrogen content of weld metal.

Key words: powder electrode; arc welding; interior porosity; diffusible hydrogen content

Weldability of Al-13.0Si-0.7Mg Alloy on T6 state TENG Yingxue[1], ZHANG Yuqi[2], GUO Jing[1], YANG Chunli[2] (1. School of Materials and Metallurgy, University of Science and Technology LiaoNing, Anshan 114001, China; 2. State Key Laboratory of Advanced Welding and Joining, Harbin Institute of Technology, Harbin 150001, China). pp 105 – 108

Abstract: Experiment of flat butt-welding is conducted on the Al-13.0Si-0.7Mg alloy on T6 state with two kinds of welding wire, ER4047 and ER5183. The process of double pulse MIG welding by both sides is used to reduce the influence of welding heat input on the base metal. The welding parameters of two welding wires are confirmed and the good weld formations are obtained. The alloy and the two wires to this alloy have good heat cracking resistance as fish-bone cracking test shows. On this basis, the microstructure observation and mechanics performance testing are conducted on the welding joints. The results show that the microstructure of joints is different for these two wires. The tensile strength of the welded joints is about 70% of the one of base metal. The hardness test indicates that there is softening phenomenon in the heat-affected zone.

Key words: Al-13.0Si-0.7Mg alloy; fish-bone cracking test; microstructure; mechanical properties

Welding thermal simulation of bainite steel used for rail way frog WANG Qiuying[1], CHEN Hui[1], HU Zhibo[2], JIANG Chao[1], LI Da[1] (1. School of Material Science and Engineering, Southwest Jiaotong University, Chengdu 610031, China; 2. China Academy of Railway Science, Beijing 100081, China). pp 109 – 112

Abstract: Gleeble-3500 was used to simulate the thermal cycle processes of bainite steel used for frog. The microstructure and properties of HAZ were investigated by optical microscopy (OM), scanning electron microscopy (SEM), transmission electron microscopy (TEM) and hardness test, respectively. The start temperature of austenite transformation, the end temperature of austenite transformation and the phase transition temperatures under different cooling rates were measured by the tangent method from the expanding curves. According to the experimental results, the simulated heat affected zone continuous cooling transforming (SHCCT) diagram of the bainite steel was constructed. SHCCT diagram provides basic data for the research of its weldability. It could be used to predict microstructure and properties of HAZ and optimize welding and repair welding processes of bainite steel frog.

Key words: bainite steel; frog; SHCCT diagram; microstructure; welding thermal simulation